Engineering Structures 300 (2024) 117191

Contents lists available at ScienceDirect

Engineering Structures

journal homepage: www.elsevier.com/locate/engstruct

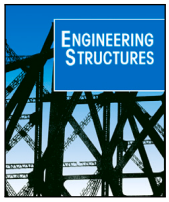

Influence of wind and seismic ground motion directionality on the dynamic response of four-legged jacket-supported Offshore Wind Turbines

Carlos Romero-Sánchez *, Luis A. Padrón

Instituto Universitario de Sistemas Inteligentes y Aplicaciones Numéricas en Ingeniería (SIANI), Universidad de Las Palmas de Gran Canaria (ULPGC), Las Palmas de Gran Canaria, 35017, Spain

ARTICLE INFO

Keywords:
Offshore wind turbine
Jacket
Soil–structure interaction
Ground motion directionality
OpenFAST

ABSTRACT

This paper aims at investigating the influence of the direction of wind and seismic ground motion on the structural response of four-legged jacket support substructures for bottom-fixed Offshore Wind Turbines located in areas with non-negligible seismic risk. To do that, a parametric analysis that considers thirteen seismic shaking directions, seven wind directions and four earthquake records is carried out. The results are presented in terms of accelerations, axial forces, bending moments and shear forces in the jacket substructure. The NREL 5 MW wind turbine supported on the jacket designed for the phase I of the OC4 project is considered. The response of the system is simulated using an OpenFAST model that takes into account multi-support seismic input, soil–structure interaction and kinematic interaction. The results show that load combinations with aligned wind and ground motion directions are never the worst-case scenario. On the contrary, the largest accelerations are found when the shaking direction acts along the side-to-side direction, and the most significant internal forces are usually found when the ground motion is aligned with one of the diagonals of the base of the jacket and not aligned with the wind direction. The paper also discusses the specific ranges of the angle of misalignment between wind and seismic shaking directions within which the maximum internal forces are expected to be found.

1. Introduction

The distance from the coast and the depth at which offshore wind farms are being installed has been increasing due to several reasons, among which one can cite the expansion of the technology and the opening of new markets, the need to avoid environmentally protected areas, or the visual pollution from Offshore Wind Turbines (OWT) installed near the coastline. Although floating wind energy is being rapidly developed, fixed-base wind turbines are still the dominant technology and a feasible possibility in many cases. In the case of significant depths, jacket support structures tend to be an option. In fact, although the monopile is clearly the preferred technology, jackets are the second preferred choice of developers (11.6% in 2021) and are expected to account for 13.4% of the near future [1].

Thus, fixed-base offshore wind turbines are moving to larger depths and, due to the expansion of the technology over the world, they are also increasingly being installed or planned in higher seismic risk areas. These two factors (depth and seismic risk) increase the relevance of Soil–Structure Interaction (SSI) on the design and on the response of the support structures of these turbines. Current standards and design guidelines state that earthquake resistance should be demonstrated for locations where seismic loads might be critical [2,3], but the experience in this field is limited because the technology is relatively recent for such sites.

The extensive research on the influence of dynamic SSI in the field of monopile-supported OWTs has repeatedly demonstrated that it significantly modifies the dynamic response of the system (see, for instance, [4–7]). Some of the strategies employed to take SSI into account in the analysis of the seismic response of monopiled offshore wind turbines are the use of: linear or non-linear springs and dashpots as part of the structural models [8–11], frequency-dependent stiffness and damping functions to represent the monopile–soil subsystem [7], Lumped Parameter Models (LPM) to fit impedance functions of monopile–soil subsystems into time-domain simulations [12,13], nonlinear Winkler p-y and Q-z springs [14–16], or finite element models of the system as a whole, including support structure, foundation and surrounding soil [17,18]. In all these studies, the foundation dynamic characteristics play a fundamental role in the overall dynamic and seismic response of the support structure and in the reduction of the damage.

The amount of research devoted to the study of the dynamic response of OWTs on jacket substructures taking SSI into account is

* Corresponding author.
E-mail addresses: carlos.romero@ulpgc.es (C. Romero-Sánchez), luis.padron@ulpgc.es (L.A. Padrón).

https://doi.org/10.1016/j.engstruct.2023.117191

Available online 22 November 2023

much more limited. The strategies used in case of jacket-supported OWTs founded on piles are, similarly to the case of monopiled OWTs: linear or non-linear springs and dashpots [19], nonlinear Winkler p-y and Q-z springs [20–22] or finite element models [23]. Thus, Alati et al. [20] analysed the response of the NREL 5 MW [24] turbine using a full model implemented in BLADED [25] and considering a jacket substructure founded on piles. The study showed that seismic loading may cause a significant increase of stress resultant demands, demonstrating the need for a seismic assessment in sites at risk from earthquakes. Later, Abhinav and Saha [26] studied the nonlinear dynamic behaviour of jacket-supported OWTs noting that ignoring SSI tends to over-estimate the ultimate strength characteristics of the OWT by 3%–60%. In addition, Abhinav and Saha [27] demonstrated the importance of SSI influence in loose sand and that the response of the jacket under dynamic loading is largely governed by the stiffness of the soil. On the other hand, Jalbi and Bhattacharya [19] developed closed-form solutions for the fundamental frequency of these jacket-supported OWTs taking SSI into account. Later, the same authors proposed a methodology for the design of the jacket substructures in the concept stage [28]. Jalbi et al. [29] also discussed the design of these structures, focused on the importance of the natural frequencies, and suggested that designer needs to optimize the configuration of the jacket and must choose the vertical stiffness of the foundation such that rocking modes of vibrations are prevented as they may interfere with the 1P frequencies of the rotor. At the same time, Gelagoti et al. [23] explored the SSI effects in OWT support structures under seismic loading. This comparative study discussed the structural behaviour of an OWT supported on a monopile and on a four-legged jacket, and the authors concluded that for the same loading combination, jackets may be more efficient in mitigating seismically induced lateral rotations than monopiles.

The effect of ground motion directionality on the seismic dynamic response of monopile supported OWTs was analysed by Mo et al. [30,31]. These studies were carried out in the time domain using OpenFAST [32] and taking into account different possible modes of operation, parked condition and normal operation. The results showed that the structural responses of the system are significantly affected by the shaking direction. They also found that bi-directional horizontal ground motion cases considering the excitation of the wind turbine in the fore–aft and side-to-side directions result in a significant underestimation of the structural responses while the environmental wind and wave loads can contribute to either mitigate or increase the effect of ground motion directionality. Jackets for OWTs subjected to different shaking directions were studied in some recent papers [33,34]. Ju and Huang [33] established an analysis framework for jacket-supported offshore wind turbines, considering some different ground motion directions (fore–aft, side-to-side and diagonal direction) and environmental loads. The results indicated that the combination of seismic and environmental loads, during power production around the rated wind speed, normally controls the design. A three-dimensional finite element model of the soil–pile–jacket–tower was developed in Abaqus by James et al. [34]. They showed the importance of considering higher modes and multi-directional ground motion, including the vertical component, on the dynamic response of offshore wind turbines. In this regard, it is also worth mentioning the study of Mroczek et al. [35] on the optimal orientation of the jacket structure. Even though seismic loads are not considered in this study, the authors analyse in detail which orientation, relative to the site specific metocean conditions, of a three-legged jacket support structure, can provide the best structural response.

Thus, the influence of wind and ground motion directionality on the dynamic and seismic response of jacket-supported OWTs, and the identification of the most demanding combination, is still an open question. For this reason, this paper aims at studying the influence of wind and seismic ground motion directionality on the structural response of the jacket support structure of offshore wind turbines and at finding out whether there exist a set of combinations of wind and shaking directions that should be paid special attention to. More specifically, the study analyses the structural response of a four-legged jacket substructure for the NREL 5 MW OWT for a set of different wind and ground motion orientations using an OpenFAST model that includes dynamic SSI and multi-support seismic input motions. Kinematic interaction is also taken into account, as the seismic input signals are filtered in order to take into account the effects of the presence of the pile foundations in the stratified soil.

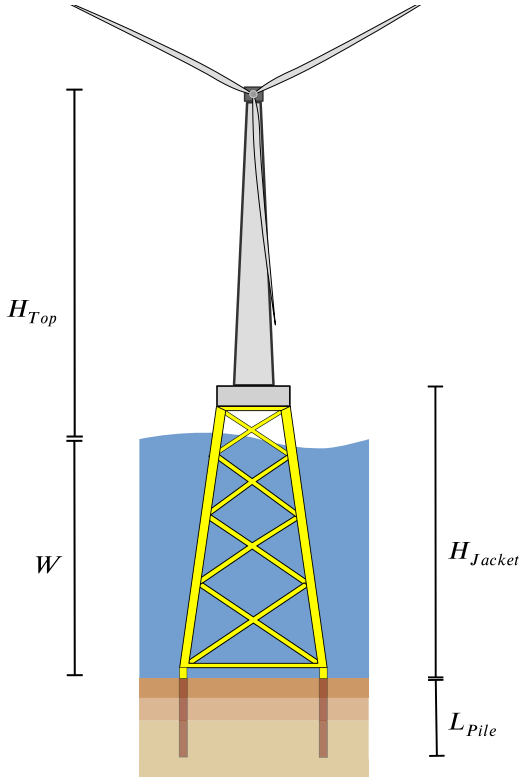

Fig. 1. General description of the jacket-supported OWT.

The present paper is structured in five sections. After the introduction, the parametric study to be performed is presented in Section 2, defining the wind turbine, the jacket substructure, the soil deposit, the seismic signals and the complete set of cases for the analysis. Once the problem has been described, the methodology for the study is presented in Section 3. Section 4 presents the most relevant results and provides a final discussion on the dynamic response of the four-legged jacket-supported OWT. Finally, a summary of the main conclusions from the manuscript is presented in Section 5.

2. Problem case description

2.1. Wind turbine and support structure

The present study on the influence of wind and seismic shaking directionality on the response of jacket-supported OWTs will be performed on the well known NREL 5 MW three-bladed turbine described in [24]. The support structure considered is the jacket support substructure designed for the phase I of the OC4 project, and described by Vorpahl et al. [36]. This four-legged jacket structure is designed using tubular members and consists of four bays. Table 1 and Fig. 1 summarize the main characteristics of the system. The material properties of the steel in the substructure are: Young's modulus $E = 210$ GPa, shear modulus $G = 80.8$ GPa, mass density $\rho = 7850\,\mathrm{kg/m^3}$ and damping ratio $\zeta = 2\%$.

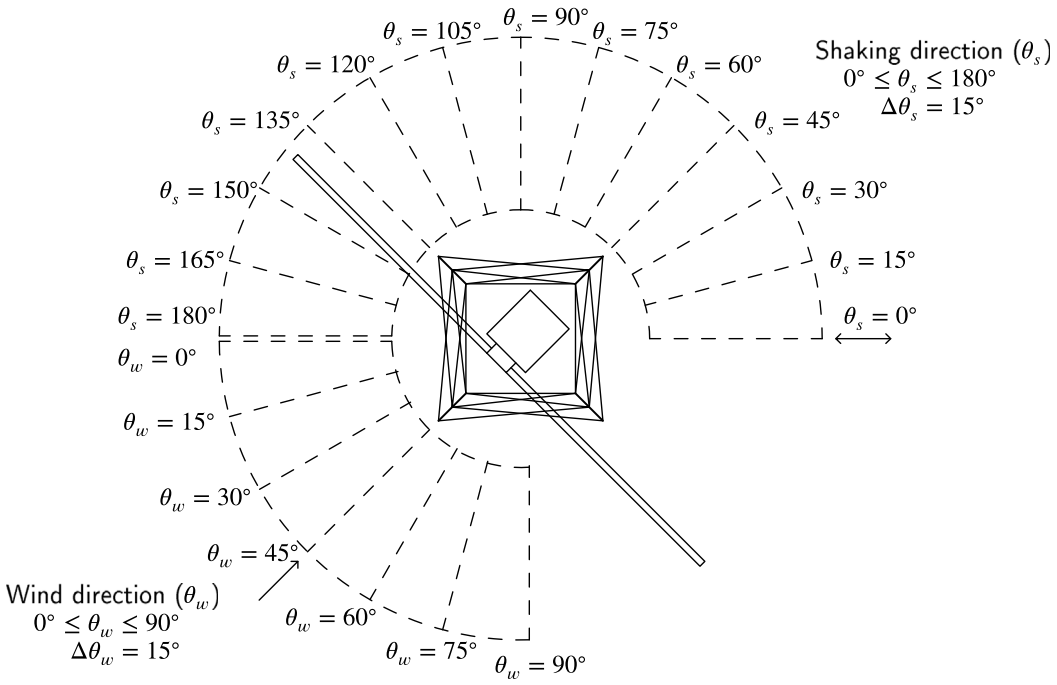

Fig. 2. Definitions of the wind and ground motion directions considered in the parametric analysis. Plan View.

Table 1
Key parameters of the OWT.

Rating [MW]	5
Rated wind speed [m/s]	11.4
Rotor diameter [m]	126
RNA mass [ton]	350
Tower top thickness [mm]	30
Tower base thickness [mm]	32
Tower top diameter [m]	4.00
Tower base diameter [m]	5.60
Tower top height from mean sea level (H_{Top}) [m]	88.15
Tower base height from mean sea level [m]	20.15
Water depth (W) [m]	50.00
Jacket height (H_{Jacket}) [m]	70.15
Number of legs	4
Top leg spacing [m]	8.00
Base leg spacing [m]	12.00
Number of bracing levels	4
Pile diameter [m]	2.082
Pile thickness [mm]	60.00
Pile depth (L_{Pile}) [m]	34.00

Table 2
Properties of the soil deposit.

Soil profile	layered
Type of soil	sand
Poisson's ratio, ν_s [-]	0.35
Density, ρ_s [kg/m^3]	2000
Shear modulus, G_s [MPa]	42.6 ($0 < z < 5$ m)
	61.9 ($5 < z < 14$ m)
	87.4 ($14 < z < \infty$)
Shear wave velocity, υ_s [m/s]	145.9 ($0 < z < 5$ m)
	175.9 ($5 < z < 14$ m)
	209.0 ($14 < z < \infty$)
Damping, ζ_s [-]	0.05

The jacket is assumed to be founded on the three-layer sandy soil deposit defined by Jonkman et al. [37] for the OC3 project. Table 2 specifies the properties of the soil profile, while the properties of the piles (summarized in Table 1) are those given by Alati et al. [20].

2.2. Set of cases for analysis

Fig. 2 presents a sketch that illustrates the parametric analysis performed in this study. Assuming a fixed orientation of the four-legged jacket support structure, the study considers a wide range of independent wind and seismic shaking directions, in such a way that a significantly high number of combinations is studied. Taking into account the quarter symmetry of the structure, the wind is assumed to blow in a 90° range, with $0° \le \theta_w \le 90°$ and $\Delta\theta_w = 15°$, thus obtaining 7 different cases for the wind direction. Simultaneously, 13 different horizontal ground motion directions are considered within a 180° range, with $0° \le \theta_s \le 180°$ and $\Delta\theta_s = 15°$. The load combinations are summarized in Table 3. The dynamic response of the substructure is analysed considering the combination of environmental loads, frequently occurring operational loads and seismic loads, following the requirements established by the design guidelines for locations where seismic actions might be critical (see for instance IEC-61400-1 [2]). Taking into account the four seismic signals described below, all different combinations result in a total of 380 simulations, including two additional cases in parked mode and without SSI. Each simulated case has a total duration of 300 s, with the earthquake ground motion starting at $t = 200$ s, after the stationary operational response of the system has already been reached. The turbine is simulated in a power production operating mode. The wind turbine remains in power production mode when the earthquake occurs, i.e., the generator continues to run normally (emergency stop is not considered). In all cases, peak responses for any given variable are computed as $R_p = \max[(R_x(t)^2 + R_y(t)^2)^{1/2}]$, where $R_x(t)$ and $R_y(t)$ are the time histories of the responses along x and y directions respectively.

Wind and wave loads are defined according to IEC 61400-3 [38]. The wind loads are computed using Turbsim for a wind speed at hub $V_{hub} = 11.4$ m/s, the rated wind speed of the turbine, and considering Normal Turbulent Model (NTM [2]), Category B turbulent wind fields and a Kaimal spectral model. The hub is always positioned according to the wind direction. Aerodyn is used to computed the aerodynamic loads on blades and tower. In all cases, it is assumed that wind and waves both act in alignment based on IEC 61400-1 [2] and DNV-OS-J101 [3]. The load combinations are defined according to Section 11.6 [2] and to DLC 11.1 [39] of the design guidelines. HydroDyn is used to calculated

Table 3
Description of the set of cases studied.

Operating mode	Wind loads	Wave loads	Earthquakes	Cases
Parked mode			No earthquake	
	Wind speed = 11.4 m/s Category B, NTM	Significant wave height = 8 m Peak-spectral period = 10 s		7
Power production	Kaimal spectrum model $0^o \leq \theta_w \leq 90°$ ($\Delta\theta_w = 15°$)	JONSWAP spectrum Aligned – Wind direction	4 earthquakes $0^o \leq \theta_s \leq 180°$ ($\Delta\theta_s = 15°$) or no earthquake	371

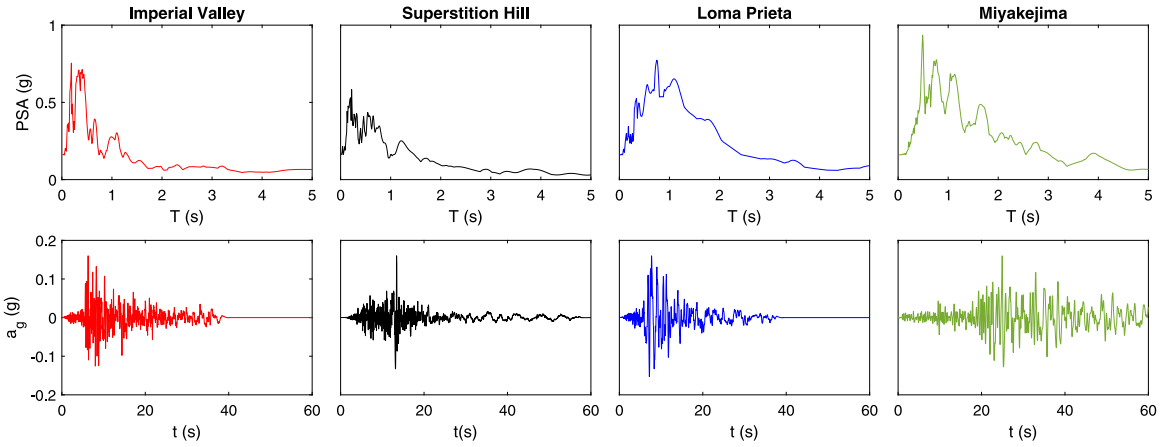

Fig. 3. Normalized pseudo-spectral accelerations (PSA) and accelerograms (a_g) of the selected seismic records.

Table 4
Information about the accelerograms.

Event name	Station name	$a_{g,max}$(g)	Observations	Database
Imperial Valley-06, 1979	Niland Fire Station	0.11	Onshore (RSN:186, Dir: 90°)	PEER
Superstition Hills-02,1987	El Centro Imp. Co. Cent.	0.36	Onshore (RSN:721, Dir: 0°)	PEER
Loma Prieta, 1984	Hollister City Hall	0.22	Onshore (RSN:777, Dir: 180°)	PEER
Miyakejima, 07/30/2000	Hiratsuka-ST1	0.19	Offshore (33.97N,139.40E, Dir: N-S)	K-NET

the wave loads. The significant height of the incident waves is 8 m. Regular and irregular waves are included.

2.3. Definition of the seismic input ground motions

In order to study the seismic response in this paper, four different accelerograms have been considered. A possible relevant factor in this type of problems is the difference between using accelerograms recorded at onshore or offshore stations (see Zhang and Zheng [40]). For this reason, and in order to evaluate the possible influence of this parameter, the four suitable accelerograms listed in Table 4 are used. Firstly, three acceleration signals from the PEER Ground Motion Database [41] where selected on the basis of the shear wave velocities at the location of the station, so that they are close to the average shear wave velocity of the soil deposit employed in this study. The selected earthquake signals were recorded by stations located over soils whose mean shear waves velocity $V_{s,30}$ is within the range from 190 to 220 m/s. Additionally, a seismic signal recorded at an offshore station was also selected from the K-NET Database [42]. All signals present relatively similar maximum ground accelerations ($a_{g,max}$). Table 4 presents the most relevant information of each recording.

Regarding the evaluation of the magnitudes of the Peak Ground Acceleration (PGA), the International Standard IEC 61400-1 [2] recommends the consideration of a 475-year recurrence period. In this study, a site within the seismic zone 2, structure's exposure level L2 and Seismic Risk Category SRC2 as defined by the ISO 19901-2 [43] is assumed. Spectral response accelerations $S_{a,map}(0.2) = 0.5$ g and $S_{a,map}(1.0) = 0.2$ g at 0.2 s and 1.0 s, respectively, are considered. These values are representative of a moderate seismic hazard, consistently with the hypothesis of linear structural behaviour and, taking into account the recurrence period mentioned above, lead to a PGA of 0.16 g. The selected recorded accelerograms are therefore normalized to this common PGA of 0.16 g, and Fig. 3 presents the normalized pseudo-spectral accelerations (PSA) and the accelerograms. These seismic signals are prescribed at free-field ground surface, and are assumed to be generated by vertically-incident far-field S-waves that produce the seismic ground motion in a particular direction for each configuration.

3. Methodology

The non-linear aero-hydro-servo-elastic code OpenFAST [32] is used herein to simulate the cases described above. In order to take into account Soil–Structure Interaction, ground input motion and Kinematic Interaction, the SubDyn module has been modified with the introduction of an LPM to represent the pile foundations embedded in the stratified soils and with the ability to consider the seismic input motion filtered by translational and rotational Kinematic Input Factors (KIFs). The impedance functions and the KIFs needed to define the systems are previously computed using a BEM–FEM model of the soil–foundation subsystem, as detailed below.

3.1. OpenFAST numerical model

The numerical tool used in this paper is based on OpenFAST [32], which is an open-source multi-physics and multi-fidelity tool for simulating the coupled dynamic response of wind turbines. This code might be considered not as a single program, but as a set of coupled computational modules, each one of them designed to simulate a specific subsystem. The different modules interact in a loosely coupled time-integration scheme, where a glue-code transfers data among modules

at each time step. This glue code is the FAST driver, that gathers all the information and drives the time-domain solution forward step-by-step using a predictor–corrector scheme.

The SubDyn module [44] was modified in order to be able to take into account dynamic soil–structure interaction and multi-support ground input motion. The input subroutine was modified to read the seismic records and the parameters of the soil–structure interaction model. The FEM subroutine and state-space formulation have been also modified. These modifications allow considering seismic loads using OpenFAST only (coupling with other software is not necessary). The code allows not only horizontal, but also vertical and rotational foundation input motion to be considered on multi-support substructures.

The equation of motion of the substructure is written as:

$$\mathbf{M}\,\ddot{\mathbf{u}}(t) + \mathbf{C}\,\dot{\mathbf{u}}(t) + \mathbf{K}\,\mathbf{u}(t) = \mathbf{F}(t) - \mathbf{M_g}\,\ddot{\mathbf{u}}_\mathbf{g}(t) - \mathbf{C_g}\,\dot{\mathbf{u}}_g(t) - \mathbf{K_g}\,\mathbf{u_g}(t) \tag{1}$$

where the expression for the effective seismic loading is obtained by separating the support motion effects from the response quantities and transferring these input terms to right hand side [45]. Thus, the motion vectors are partitioned to separate the response quantities from the input: $\mathbf{u}(t)$ includes the degrees of freedom of the structure and $\mathbf{u_g}(t)$ contains the components of the foundation input motions at each support. The dots represent differentiation with respect to time. The global mass, damping and stiffness matrices have been partitioned accordingly. $\mathbf{F}(t)$ represents the external forces acting at each degree of freedom of the structure. In contrast to the original SubDyn module which assumes a fixed base, the new approach considers that the vector of displacements at the boundary nodes, $\mathbf{u_R}(t)$, contains the displacements at the interface node with the tower, $\mathbf{u_I}(t)$, and the displacements at base nodes, which would move following the ground motion vector.

$$\mathbf{u}_R(t) = \begin{pmatrix} \mathbf{u}_g(t) \\ \mathbf{u}_I(t) \end{pmatrix} \tag{2}$$

The beam elements in the jacket substructure are modelled as Timoshenko three-dimensional beams, and discretized using two-nodes 12 degrees of freedom finite elements defined by the corresponding stiffness and mass matrices, considering linear response and rigid joints. On the other hand, the Craig–Bampton method is used to reduce the number of the internal generalized degrees of freedom of the substructure. Taking all this into account, the general equation of motion is transformed and the derived matrices are partitioned, so that one can write:

$$\begin{bmatrix} \tilde{\mathbf{M}}_{BB} & \tilde{\mathbf{M}}_{Bm} \\ \tilde{\mathbf{M}}_{mB} & I \end{bmatrix} \begin{pmatrix} \ddot{\mathbf{u}}_I(t) \\ \ddot{\mathbf{q}}_m(t) \end{pmatrix} + \begin{bmatrix} \tilde{\mathbf{C}}_{BB} & \tilde{\mathbf{C}}_{Bm} \\ \tilde{\mathbf{C}}_{mB} & \mathbf{C}_{mm} \end{bmatrix} \begin{pmatrix} \dot{\mathbf{u}}_I(t) \\ \dot{\mathbf{q}}_m(t) \end{pmatrix} + \begin{bmatrix} \tilde{\mathbf{K}}_{BB} & 0 \\ 0 & \mathbf{K}_{mm} \end{bmatrix} \begin{pmatrix} \mathbf{u}_I(t) \\ \mathbf{q}_m(t) \end{pmatrix} = \begin{pmatrix} \tilde{\mathbf{F}}_{tp}(t) \\ \tilde{\mathbf{F}}_m(t) \end{pmatrix} - \begin{bmatrix} \mathbf{M}_{Ib} \\ \mathbf{M}_{mb} \end{bmatrix} \ddot{\mathbf{u}}_g(t) - \begin{bmatrix} \mathbf{C}_{Ib} \\ \mathbf{C}_{mb} \end{bmatrix} \dot{\mathbf{u}}_g(t) - \begin{bmatrix} \mathbf{K}_{Ib} \\ \mathbf{K}_{mb} \end{bmatrix} \mathbf{u}_g(t) \tag{3}$$

where $\mathbf{M}_{[..]}$, $\tilde{\mathbf{M}}_{[..]}$, $\mathbf{C}_{[..]}$, $\tilde{\mathbf{C}}_{[..]}$, $\mathbf{K}_{[..]}$ and $\tilde{\mathbf{K}}_{[..]}$ are the resulting mass, damping and stiffness submatrices, which are computed during initialization; $\mathbf{q}_m(t)$ and $\tilde{\mathbf{F}}_m(t)$ represent the displacements and the external forces at the interior nodes approximated by a subset of the interior generalized DOFs; and $\tilde{\mathbf{F}}_{tp}(t)$ are the forces at the transition piece. The right-hand side of the equation shows the external forces on the substructure and the effective seismic loading. State-space formulation of the substructure structural dynamic is used to integrate SubDyn into the FAST driver. The equation of motion is cast into standard linear system state equation of the form:

$$\dot{\mathbf{x}}(t) = \mathbf{A}\mathbf{x}(t) + \mathbf{B}\mathbf{u}(t) + \mathbf{F}_x(t) \tag{4}$$

where $\mathbf{A}$ and $\mathbf{B}$ are matrices of constants coefficients.

The implementation of the multi-support input motion and of the dynamic soil–structure interaction model have been verified by comparison against results obtained from a finite-elements beam model of the offshore wind turbine without wind or waves. More details about the modifications and the verification cases are described in Romero-Sánchez and Padrón [46]. The code is available in OpenFAST version 3.0.0 and can be downloaded at: https://github.com/mmc-siani-es/openfast_3.0.0_multisupport.

Table 5
OWT Natural frequencies.

	Fixed-base model	Flexible-base mode
1st side-to-side mode	0.314 Hz (3.18 s)	0.302 Hz (3.31 s)
1st fore–aft mode	0.316 Hz (3.16 s)	0.300 Hz (3.33 s)
2nd side-to-side mode	1.165 Hz (0.86 s)	0.987 Hz (1.01 s)
2nd fore–aft mode	1.213 Hz (0.82 s)	0.949 Hz (1.05 s)

3.2. Soil–structure interaction and seismic action modelling

The impedance of the soil–foundation subsystem is introduced in the model through individual simplified Lumped Parameter Models for each pile foundation at the base of each leg. The mathematical details of this LPM are described in Carbonari et al. [47], while the details about its implementation into SubDyn can be found in Romero-Sánchez and Padrón [48]. This LPM configuration allows to model and fit the translational $K_{xx}(\omega)$, rotational $K_{\theta\theta}(\omega)$ and coupled horizontal-rocking $K_{x\theta}(\omega)$ complex-valued impedance functions simultaneously, while the spring–damper model is adopted for vertical $K_{zz}(\omega)$ and torsional $K_t(\omega)$ impedances. It also allows to introduce the most relevant aspects of these frequency-domain impedance functions into the time-domain simulation of the whole system in OpenFAST.

The lateral and rotational KIFs quantify the filtering effect that the presence of the foundation produce over the incoming seismic waves. Thus, these complex-valued frequency-domain factors $I_u(\omega)$ and $I_\theta(\omega)$ are defined as the ratio between the pile head displacement or rotation and the free-field motion. To obtain these functions, the embedded portion of a single pile, in the soil profile under consideration, is assumed to be subjected to vertically-incident S-waves. The standard Frequency Domain Method of response [49] is employed to filter the earthquake signals according to these KIFs.

Impedance functions and KIFs are all computed using the numerical model described by Álamo et al. [50] for the dynamic analysis of pile foundations in complex soil profiles. This model is based on the use of the integral expression of the reciprocity theorem together with specific Green's functions for a viscoelastic layered half-space for representing the soil behaviour, including its radiation and material damping.

Table 5 presents the first and second side-to-side (SS) and fore–aft (FA) natural frequencies of the system, obtained from the SS and FA accelerations at the tower top, when the wind turbine is in parked conditions and subjected to environmental loads. These computed values are very close to those obtained by Alati et al. [20] for this case. In order to show the relevance of soil–structure interaction, these natural frequencies are listed considering both fixed-base and flexible-base models. As expected, soil–structure interaction plays a significant role in the reduction of the natural frequency, causing, for instance, a 5% reduction in the fore–aft fundamental frequency.

In Fig. 4, these natural frequencies are presented on top the acceleration response spectra of the considered earthquakes. This figure highlights the fact that, even though all four seismic signals have been normalized to a common peak ground acceleration, the spectral values for the different earthquakes differ significantly around both natural frequencies. In most cases, the largest spectral values are found for the Loma Prieta signal, while the lowest are found for the Superposition Hill record. These observations will have an impact on the different functions that will be analysed later.

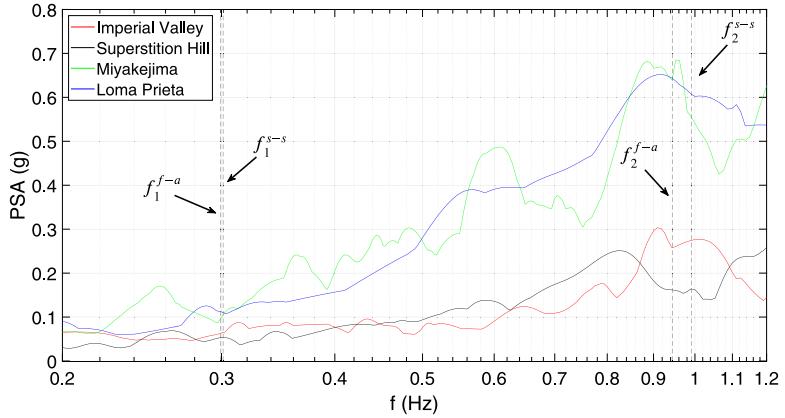

Fig. 4. Acceleration response spectra of the seismic signals considered and first and second natural frequencies of the structural system.

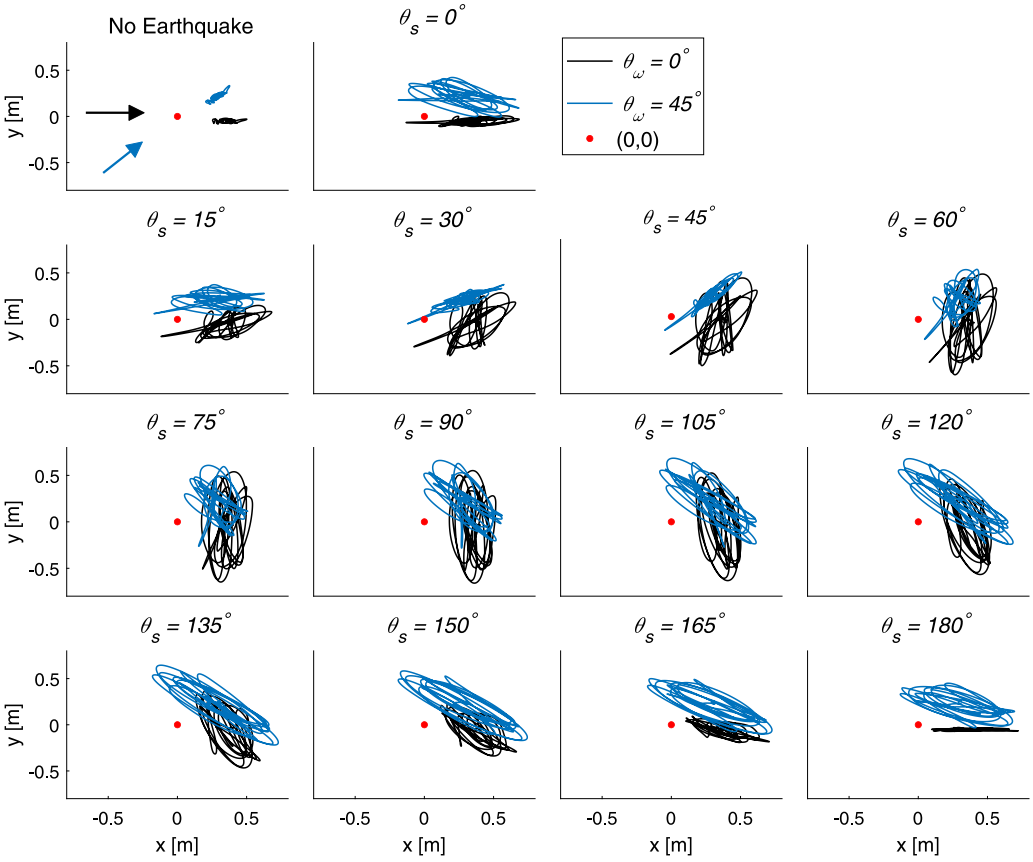

Fig. 5. Trajectories at the tower top during the seismic shaking, for the Loma Prieta seismic input and for $\theta_w = 0°$ and 45°.

4. Results

4.1. General response and tower top trajectories in different scenarios

The influence of the different load scenarios described in Section 2 can be qualitatively understood from Fig. 5, where the trajectories of tower top under the thirteen different ground motion directions for the Loma Prieta earthquake signal, and two wind directions, are depicted. The motions corresponding to the $\theta_w = 0°$ and 45° incoming wind directions are plotted in black and blue curves, respectively, and two arrows of the same colours are included in the first plot (in absence of earthquake) to represent such wind directions. The red dot represents the initial position of the tower top in unloaded conditions. In all cases, the motions are plotted between $t = 200$ and $t = 240$ s, coinciding with the duration of the seismic shaking.

These plots provide a sense on how the structural system is responding at the different configurations. When wind and seismic shaking directions are aligned (cases $\theta_w = 0°$ and $\theta_s = 0°$ or 180°, or $\theta_w = \theta_s = 45°$) the trajectories are located along an elongated area. As expected, motions describe a wider area when wind and seismic ground motion directions are misaligned. The major axis of the ellipse drawn during the motions tend to be oriented with the shaking direction, for this particular seismic input. When wind and ground motion direction are perpendicular (for instance, for $\theta_w = 0°$ and $\theta_s = 90°$) trajectories describe the largest area. In this regard, it is also observed that the amplitude of the excursion due to the seismic shaking (the length of the major axis of the ellipse) when wind and ground motion direction

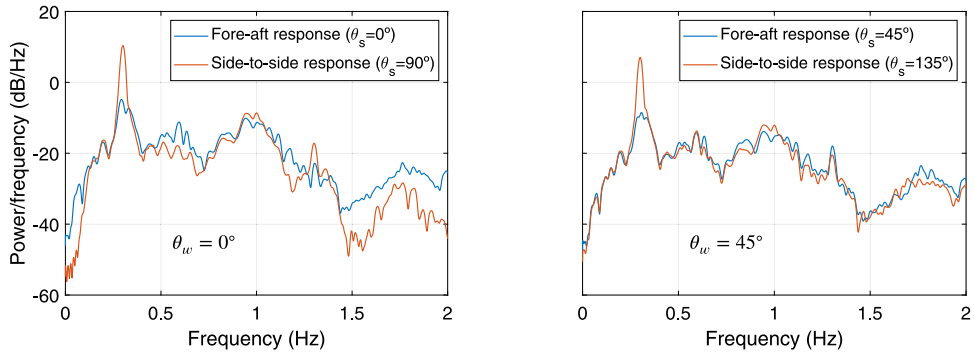

Fig. 6. Power Spectral Densities obtained from the tower top accelerations in power production conditions, under the Loma Prieta seismic input and for $\theta_w = 0°$ and 45°.

are perpendicular is significantly larger that the excursion due to the seismic shaking when wind and ground motion are aligned. This is because, in the first case, the shaking takes place in the side-to-side direction, for which the aeroelastic damping is much smaller than in the fore–aft direction. Another way to analyse the influence of the aeroelastic damping is to perform a frequency domain comparison. Fig. 6 presents the Power Spectral Densities obtained from the tower top accelerations under power production conditions. The wind direction is considered in two different cases ($\theta_w = 0°$ and 45°) and the Loma Prieta earthquake acts in fore–aft and side-to-side directions. As expected, the accelerations signals in fore–aft direction (blue line) are more damped than in the side-to-side direction. This phenomenon is due to the aeroelastic damping induced by the sweeping rotor in the fore–aft direction when the wind turbine is in operational conditions. This observation will be relevant later to provide some insight on how internal forces evolve for the different configurations. It is also worth noting that, in absence of seismic input and for both wind directions, the trajectories of the tower top are not exactly aligned with the undeformed (0,0) position due to the fact that the rotor is rotating and its effects are not symmetrical in the side-to-side direction.

4.2. Influence of ground motion directionality and seismic input signal

To study the influence of ground motion directionality and seismic input signal, Fig. 7 shows the peak responses of accelerations and several internal forces for all earthquake considered in this study. Specifically, the peak accelerations obtained at the transition piece, and the peak bending moments, axial and shear forces at specific nodes of the jacket substructure, are presented for all shaking directions in polar plot format. Results for $\theta_w = 0°$ and 90° are considered. A different colour has been used for each earthquake, considering the same colours as in Fig. 3. The internal forces are presented, for each case, at the jacket node where the highest peak value is registered for each one of the variables. In this regard, Fig. 8 illustrates the locations at which the peak internal forces are found. The nodes where the peak axial forces are developed are located near the bottom of the jacket legs, at the joint with the bottom bracing, while the greatest shear forces arise at the nodes of the upper part of the jacket legs, at the joint with the upper bracing. Finally the highest bending moments can be found at the nodes where the jacket is connected to each pile head, at mudline level. The descriptions of these locations hold true for all configurations even though the specific leg, among the four legs of the jacket, at which the peak value is located in every case, will obviously depend on the directions of wind and seismic shaking.

Fig. 7 shows that the evolutions observed for the different variables as a function of the ground motion direction θ_s are qualitatively equivalent among the different earthquakes considered, but the magnitude of the effects of each one of the seismic signals is clearly different. The Loma Prieta is the input signal that produces the largest accelerations and internal forces, while the Superstition Hill record generates significantly smaller effects. This is due to the differences found in the response spectra of the different earthquakes, especially around the natural frequencies of the system, as described in Section 3.2 (see Fig. 4). Thus, the shape of the polar plot for a particular variable and wind direction is common to the four earthquakes, although the scales change.

The evolution of the peak accelerations at the transition piece with the seismic shaking direction is quasi-symmetrical about the 90° axis. The maximum accelerations occur when the directions of wind and ground motion are perpendicular to each other (i.e., when the shaking acts along the side-to-side direction) and the minimum accelerations occur when both directions are aligned (i.e., when the shaking acts along the fore–aft direction). This is the expected behaviour, as aerodynamic damping is always much smaller in the side-to-side direction. Differences in these peak accelerations due to the ground motion directionality can reach percentages of 20%.

The evolution of the internal forces with the shaking direction is less symmetrical. Different from the previous case, where maximum peak accelerations at the transition piece arose for $\theta_s = 0°$ and 90° along the side-to-side directions, maximum peak internal forces develop, in most cases, for $\theta_s = 45°$ or 135° for any of the two considered wind directions. Minimum peak values are often found for $\theta_s = 0°$, 90° or 180°, especially in the case of axial forces. Regarding the bending moments, an intersection between the curves corresponding to $\theta_w = 0°$ and 90° is produced when the shaking acts at 45° for all earthquakes. The highest peak response is produced at $\theta_s = 135°$. The shapes of the polar curves, specially those of axial forces and shear forces, are evidently due to the relative orientation between the layout of the base of the structure and the direction defined as 0°, with a 45° angle between $\theta_w = 0°$ and the diagonal between legs (see Fig. 2). It is also clear from the results that, as expected, ground motion directions of 0° or 180° are not equivalent. Also, the polar plots obtained for the shear force for $\theta_w = 0°$ and 90° are almost identical, while the rest of response functions show a significant dependence on wind direction.

4.3. Influence of wind direction

Fig. 9 presents the evolution of the peak axial forces and bending moments at the nodes mentioned above (see Fig. 8) for all wind directions. Again, shaking direction is represented in the polar axis while, in this case, the different curves represent the different wind directions. In order to focus on the influence of wind direction on the system response, results are presented for only one seismic signal (Loma Prieta).

In this case, both peak axial forces and peak bending moments tend to reach the maximum values for $\theta_s = 135°$ and $\theta_w = 0°$, with these internal force decreasing for increasing θ_w for this shaking direction. However, this trend, as a function of θ_w, is not common to all ground motion directions and is almost the opposite, for instance, for $\theta_s = 0°$. At $\theta_s \simeq 45°$, a crossing between the wind lines is observed for the peak

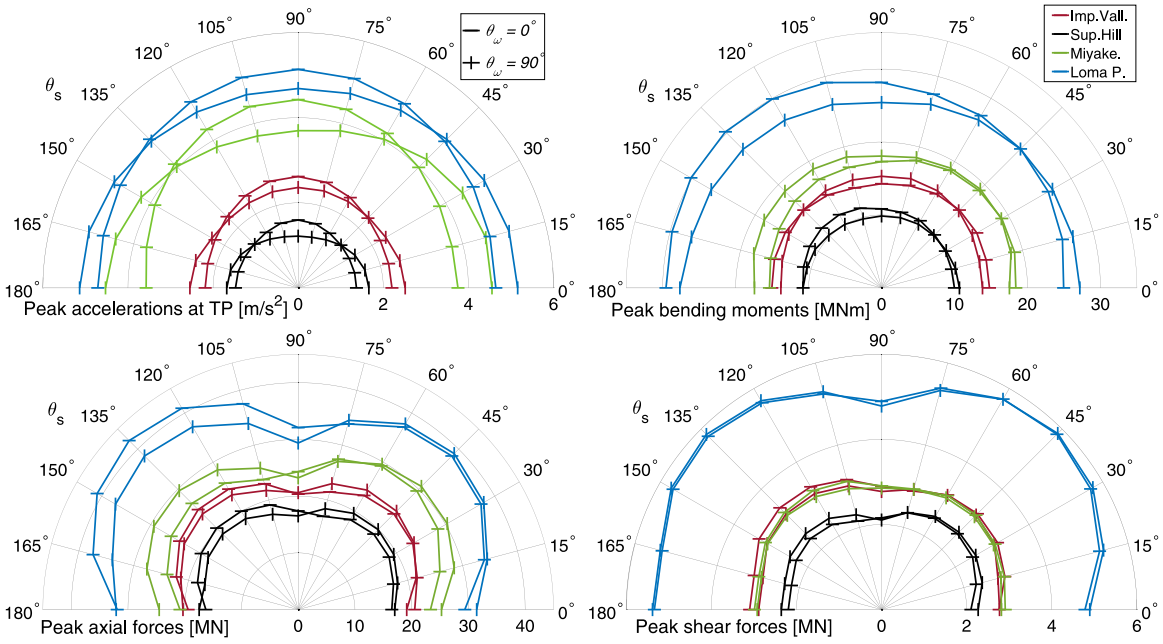

Fig. 7. Influence of seismic shaking direction on the peak response values in terms of accelerations at the transition piece, and of bending moments, axial and shear forces for $\theta_w = 0°$ and 90°.

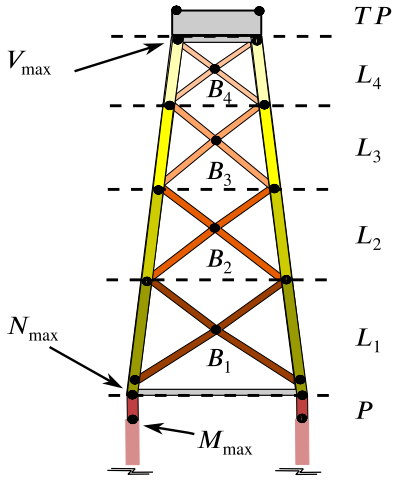

Fig. 8. Locations at which the different peak internal forces in the jacket substructure arise.

bending moments, while this point of crossing moves to $\theta_s \simeq 75°$ in the case of the axial forces. As mentioned above, the location of the maximum axial forces is affected by the geometry and orientation of the jacket, since the highest peak responses are found in this case when the earthquake acts in the direction of one of the supports.

The analysis of the results in terms of not only peak values, but also root mean square (rms) values, is useful to understand whether the observed trends are consistent along the responses, and are not only representative of isolated peaks. For this reason, Fig. 10 presents the rms values in terms of axial forces and bending moments, under the Loma Prieta earthquake, in such a way that the format of the figure is equivalent to that of Fig. 9. Here, rms values are computed along the significant duration of each seismic signal is presented. The common D_{a595} significant duration [51] is considered, which is defined as the time interval between 5%–95% of the Arias intensity [52]. The comparison between Figs. 9 and 10 shows that the conclusions that can be drawn in terms of both measures are equivalent to each other. The shape and relative magnitudes of the curves is comparable though, of course, magnitudes are different.

In order to examine more closely the influence of wind direction, Fig. 11 shows the variation of internal forces according to some particular ground motion direction for all seismic signals considered in this paper. The x-axis presents the 7 wind directions used, and each line of different colour represents one representative direction of the shaking. In this case, five relevant directions have been considered, specifically, $\theta_s = 0°$, 45°, 90°, 135° and 180°.

No clear common trends are observed between the different earthquakes or directions. However, some interesting conclusions can be drawn from these results. Firstly, the extend of the variation in the computed internal forces is generally larger for different ground motion directions than for different wind directions. In other words, the direction of the seismic shaking tends to have a larger influence on the span of these variables than wind direction. This is particularly so when studying shear forces. However, this is not always true, especially when looking at the axial forces, as the variations produced by shaking or wind directions are similar when the Superstition Hill earthquake is considered. Secondly, maximum peak axial forces and peak shear forces are always found for $\theta_s = 45°$ or 135° (orange and purple lines, respectively). This occurs for all wind directions. In the case of bending moments, this observation does not always hold true, as $\theta_s = 180°$ yields higher bending moments in Superstition Hill and Loma Prieta earthquakes when $\theta_w \geq 30°$. Finally, different behaviours are observed for different earthquakes, with only some exceptions where similar trends can be observed, and with the trends in the results for the Miyakejima earthquake (the only offshore recording) being different from any of the other cases. Thus, the need for considering always different seismic signals of different origins is clear.

4.4. Influence of the misalignment between ground motion and wind directions

After having studied the influence of wind and seismic shaking directions (in absolute terms) on the evolution of peak internal structural forces in the jacket substructure, it is interesting to analyse now the influence of the misalignments $\Delta = \theta_w - \theta_s$ between ground motion and wind directions. To do so, Fig. 12 illustrates the way in which the mean

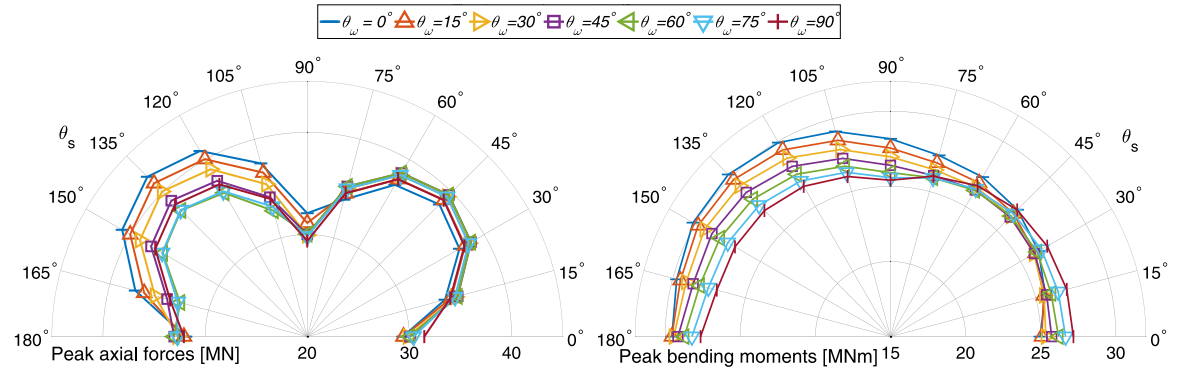

Fig. 9. Peak response values in terms of axial forces and bending moments in the jacket substructure under the Loma Prieta earthquake for all seismic shaking and wind directions.

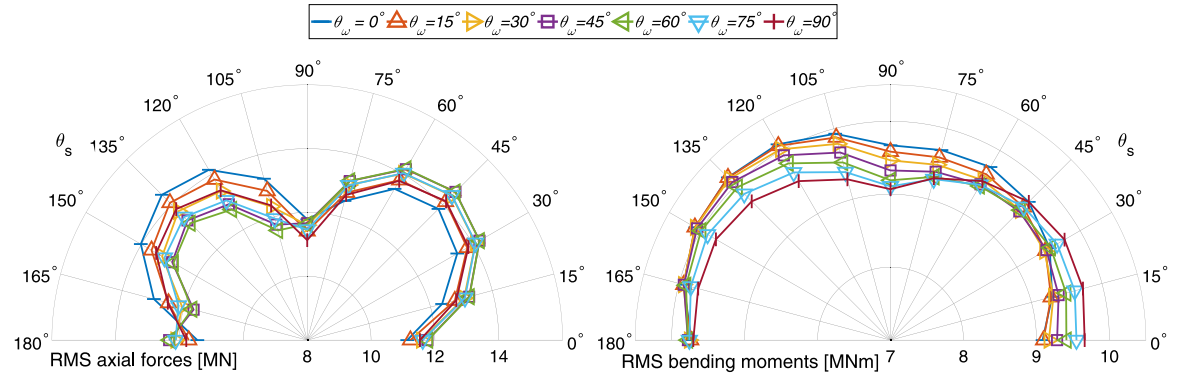

Fig. 10. Root-means-square values in terms of axial forces and bending moments in the jacket substructure under the Loma Prieta earthquake for all seismic shaking and wind directions.

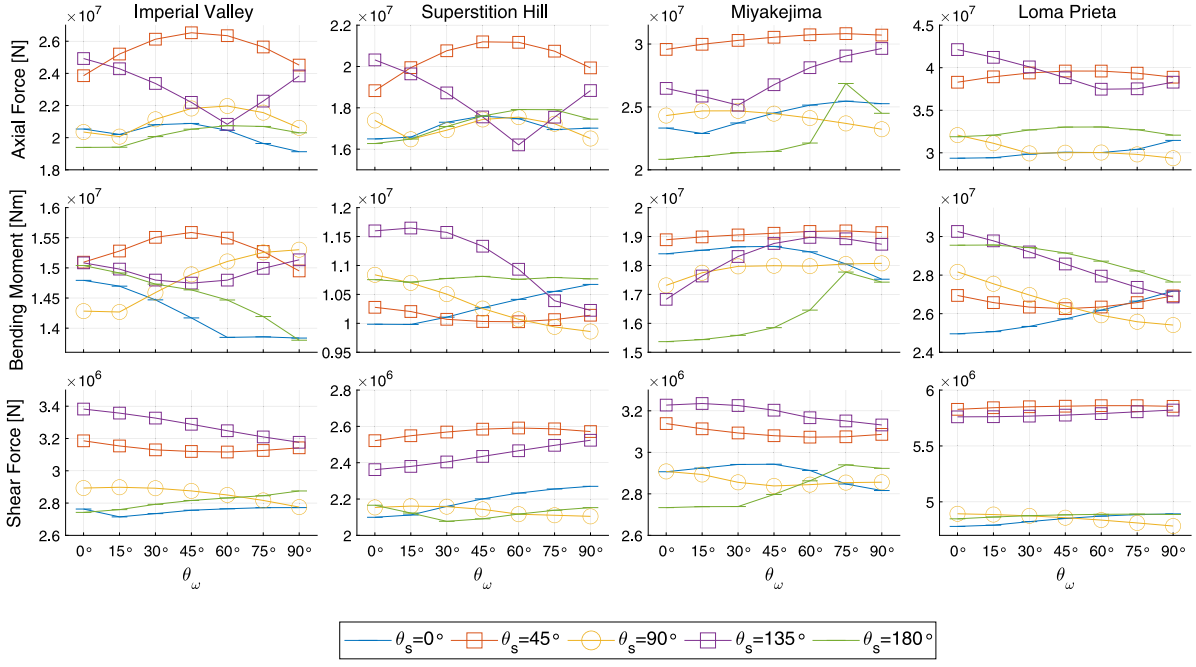

Fig. 11. Influence of wind direction on the peak response values in terms of axial forces, bending moments and shear forces in the jacket substructure for all earthquakes.

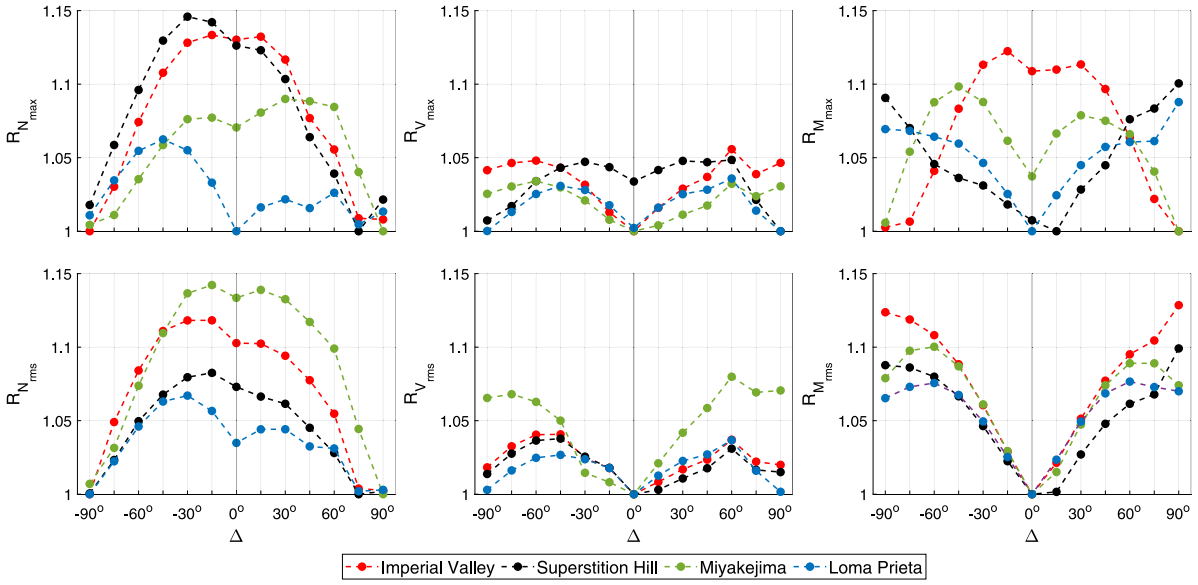

Fig. 12. Amplification ratios for axial forces, shear forces and bending moments for different misalignment angles between wind and ground motion direction.

peak or rms values of the three considered internal forces vary for the different misalignment values. For this purpose, results are presented in terms of the following amplification ratios:

$$\mathrm{R}_{X_{\max}}(\Delta) = \frac{\sum_{i=1}^{n}\left[X_{max}\left(\theta_{w_i}, \Delta+\theta_{w_i}\right)\right]/n}{\min_{\Delta}\left[\sum_{i=1}^{n}\left[X_{max}\left(\theta_{w_i}, \Delta+\theta_{w_i}\right)\right]/n\right]} \tag{5}$$

$$\mathrm{R}_{X_{\mathrm{rms}}}(\Delta) = \frac{\sum_{i=1}^{n}\left[X_{rms}\left(\theta_{w_i}, \Delta+\theta_{w_i}\right)\right]/n}{\min_{\Delta}\left[\sum_{i=1}^{n}\left[X_{rms}\left(\theta_{w_i}, \Delta+\theta_{w_i}\right)\right]/n\right]} \tag{6}$$

where $X_{\max}$ can be peak axial forces $N_{\max}(\theta_w, \theta_s)$, shear forces $V_{\max}(\theta_w, \theta_s)$ or bending moments $M_{\max}(\theta_w, \theta_s)$ for a given combination of ground motion and wind directions; X_{rms} can be root-mean-square values of axial forces $N_{\mathrm{rms}}(\theta_w, \theta_s)$, shear forces $V_{\mathrm{rms}}(\theta_w, \theta_s)$ or bending moments $M_{\mathrm{rms}}(\theta_w, \theta_s)$ for a given combination of ground motion and wind directions, and at the same member at which the peak values are found for each combination; and $n = 7$ is the number of combinations for any given Δ. This amplification factors provide information on how the peak or rms values found for a given combination of seismic shaking and wind directions with a certain misalignment between them relate to the case in which such misalignment angle yields the smallest forces among all of them.

The results show that the load combination that considers aligned wind and ground motion actions ($\Delta = 0°$) is never the worst-case scenario. This observation is in line with what was found by Mo et al. [30,31] for monopiled OWTs. On the contrary, the misalignment values for which the highest forces are found tend to be $15° \leq |\Delta| \leq 45°$ for the axial forces, $45° \leq |\Delta| \leq 75°$ for the shear forces, and $|\Delta| = 90°$ or $15° \leq |\Delta| \leq 45°$ for the bending moments, depending on the specific earthquake.

4.5. General trends considering wind and ground motion direction simultaneously

Another relevant factor to analyse within this study is how much the internal forces increase with the arrival of an earthquake. In order to quantify the significance of the seismic shaking, Fig. 13 shows the amplification ratios between the results computed taking into account, or disregarding (NS: Non-Seismic), the earthquake input, maintaining always the mode of operation in normal production. The horizontal axis denotes each one of the different wind direction considered, hence the direction of the hub. The different symbols represent the ground motion direction and the colours represent the four seismic signal considered. Left and right plots present the results in terms of axial forces or bending moments, respectively.

A first observation is that all amplification ratios are significantly higher than the unit ratio, which illustrates the relevance of the seismic actions in terms of the peak forces developed along the jacket support structure. The specific value depends on the earthquake signal and on the wind and ground motion directions, with ratios over 4 for axial forces and 7 for bending moments, for the Loma Prieta earthquake. Bending moments are more affected by the seismic loads. In the case of the axial forces, the highest ratios occur when wind directions are $\theta_w = 0°$ or 90°, and the ground motion direction is $\theta_s = 45°$. In the case of bending moments, the trends are not so clear with respect to wind direction, but the highest ratios are found, as mentioned above, when the shaking occurs in the side-to-side direction in each case.

Finally, and after having analysed in the detail the evolutions of the internal forces, Fig. 14 presents the rms values for the acceleration at the tower top considering all ground motion directions in the polar plot, and one curve for every wind direction, for the Loma Prieta earthquake.

As expected, maximum accelerations are found, again, when the shaking occurs along the side-to-side direction in each case. The evolution of the amplitudes is clear, with the smaller amplitudes arising when both actions are aligned, and increasing amplitudes of response when the shaking acts with larger angles of misalignment with respect to the wind direction. This tendency is due to the variability in the aeroelastic damping, and was already observed in Fig. 5.

5. Conclusions

The present research has looked into the influence of wind and seismic shaking directionality on the dynamic structural response of jacket-type support substructures for Offshore Wind Turbines located in areas with non-negligible seismic risk. To do that, a parametric study that included 13 seismic ground motion directions and 7 wind directions was carried out. Four different earthquake records were employed, and results were presented in terms of accelerations, bending moments, axial forces and shear forces in the jacket substructure. The response of the NREL 5 MW Offshore Wind Turbine on the jacket substructure defined for the phase I of the OC4 project was simulated using an OpenFAST model that included soil–structure interaction and multi-support input motion. Kinematic interaction was also taken into account, as the seismic input signals were filtered in order to take

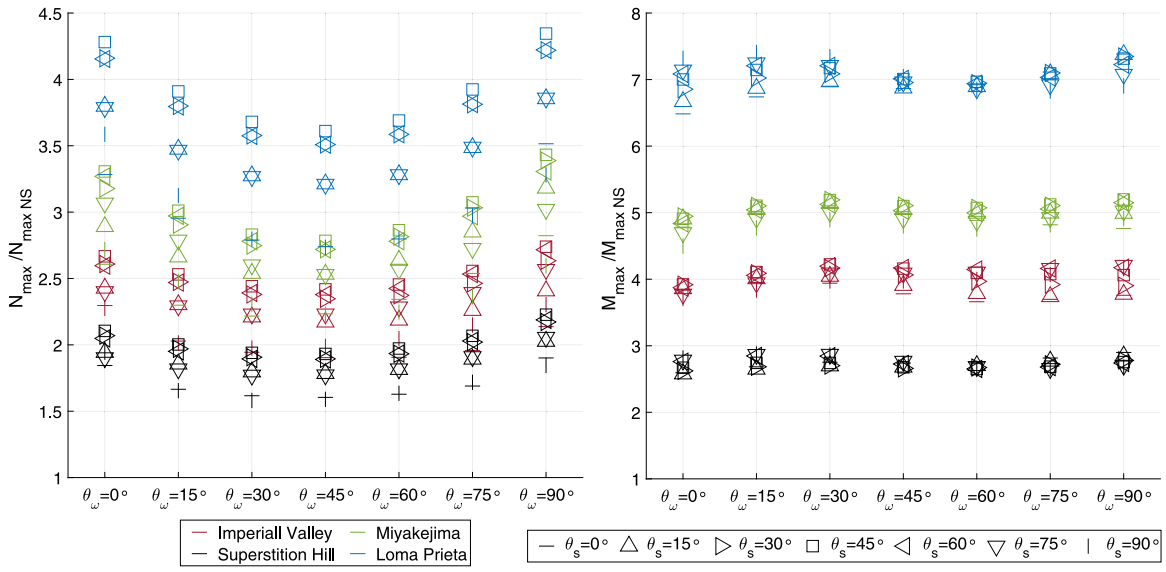

Fig. 13. Ratios between peak seismic response and peak non-seismic response of axial forces and bending moments in the jacket substructure.

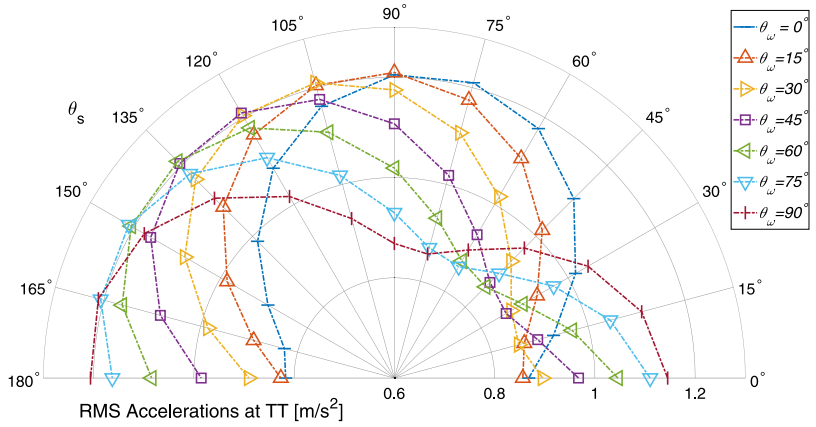

Fig. 14. Root-means-square values of accelerations at tower top for all ground motion and wind directions for the Loma Prieta seismic record.

into account the effects of the presence of the pile foundations in the stratified soil. The turbine was assumed to be in power production mode.

It was found that, due to aeroelastic damping (which is much higher in the fore–aft direction than in the side-to-side direction) the amplitude of the vibrations is much more relevant when the seismic shaking acts along the side-to-side direction, in comparison to the situation in which it acts along the fore–aft direction. However, due to the geometry of the jacket, the conclusion is not the same when looking at the internal forces. In this case, the maximum internal forces are usually found when the ground motion is aligned with the direction of the diagonal of the base of the jacket structure and not aligned with the wind direction. It is also worth noting that the seismic shaking direction tends to have a larger influence on the peak internal forces than wind direction. This is particularly so when studying shear forces.

In any case, it is clear that the load combinations that assume aligned wind and ground motion directions are never the worst-case scenario. On the contrary, the misalignment values for which the highest forces are found tend to be $15° \leq |\Delta| \leq 45°$ for the axial forces, $45° \leq |\Delta| \leq 75°$ for the shear forces, and $|\Delta| = 90°$ or $15° \leq |\Delta| \leq 45°$ for the bending moments. These ranges provide a relatively narrow margin within which the worst-case scenario combination can be found, although a specific combination cannot be specified for all cases. This is partly so because the combinations for which the maximum peak values are found vary, within these ranges, with different earthquakes. Consequently, a sufficiently large set of seismic signals (ideally including also offshore stations) and of combinations of ground motion and wind directions must be taken into account during the phases of detailed design of jacket substructures for Offshore Wind Turbines located in areas with sufficiently high level of seismic risk.

CRediT authorship contribution statement

Carlos Romero-Sánchez: Conceptualization, Methodology, Software, Validation, Formal analysis, Investigation, Writing – original draft, Writing – review & editing, Visualization, Supervision, Funding acquisition. **Luis A. Padrón:** Conceptualization, Methodology, Software, Validation, Formal analysis, Investigation, Writing – original draft, Writing – review & editing, Visualization, Supervision, Funding acquisition.

Declaration of competing interest

The authors declare that they have no known competing financial interests or personal relationships that could have appeared to influence the work reported in this paper.

Data availability

Data will be made available on request.

Acknowledgements

This research was funded by the Ministerio de Ciencia, Innovación *y* Universidades and the Agencia Estatal de Investigación of Spain (MCIN/AEI/10.13039/501100011033) and FEDER through research project PID2020-120102RB-I00 and by Consejería de Economía, Conocimiento *y* Empleo (Agencia Canaria de la Investigación, Innovación *y* Sociedad de la Información) of the Gobierno de Canarias and FEDER, Spain through research project ProID2020010025. In addition, C. Romero-Sánchez is a recipient of the research fellowship (TESIS2022 010011), from the Program of predoctoral fellowships from the Consejería de Economía, Conocimiento *y* Empleo (Agencia Canaria de la Investigación, Innovación *y* Sociedad de la Información), Spain of the Gobierno de Canarias and Fondo Social Europeo. The authors are grateful for this support.

References

[1] Musial W, Spitsen P, Duffy P, Beiter P, Marquis M, Hammond R, et al. Offshore wind market Report: 2022 edition. Technical report, National Renewable Energy Lab.(NREL), Golden, CO (United States); 2022.
[2] IEC. 61400-1:2020 Wind energy generation systems - Part 1: Design requirements. International Electrotechnical Commission; 2020.
[3] DNV. Design of offshore wind turbine structures. Offshore standard DNV-OS-J101. DetNorske Veritas AS; 2014.
[4] Lombardi D, Bhattacharya S, Wood DM. Dynamic soil–structure interaction of monopile supported wind turbines in cohesive soil. Soil Dyn Earthq Eng 2013;49:165–80.
[5] Zania V. Natural vibration frequency and damping of slender structures founded on monopiles. Soil Dyn Earthq Eng 2014;59:8–20.
[6] Álamo GM, Aznárez JJ, Padrón LA, Martínez-Castro AE, Gallego R, Maeso O. Dynamic soil-structure interaction in offshore wind turbines on monopiles in layered seabed based on real data. Ocean Eng 2018;156:14–24.
[7] Medina C, Álamo GM, Quevedo-Reina R. Evolution of the seismic response of monopile-supported offshore wind turbines of increasing size from 5 to 15 MW including dynamic soil-structure interaction. J Mar Sci Eng 2021;9(11):1285.
[8] Bazeos N, Hatzigeorgiou GD, Hondros ID, Karamaneas H, Karabalis DL, Beskos DE. Static, seismic and stability analyses of a prototype wind turbine steel tower. Eng Struct 2002;24:1015–25.
[9] Stamatopoulos GN. Response of a wind turbine subjected to near-fault excitation and comparison with the Greek aseismic code provisions. Soil Dyn Earthq Eng 2013;46:77–84.
[10] Krathe VL, Kaynia AM. Implementation of a non-linear foundation model for soil-structure interaction analysis of offshore wind turbines in FAST. Wind Energy 2016;20(4):695–712.
[11] Løken Ingrid B, Kaynia Amir M. Effect of foundation type and modelling on dynamic response and fatigue of offshore wind turbines. Wind Energy 2019;22(12):1667–83, arXiv:https://onlinelibrary.wiley.com/doi/pdf/10.1002/we.2394.
[12] Padrón LA, Carbonari S, Dezi F, Morici M, Bordón JDR, Leoni G. Seismic response of large offshore wind turbines on monopile foundations including dynamic soil–structure interaction. Ocean Eng 2022;257:111653.
[13] Damgaard M, Zania V, Andersen Lars V, Ibsen LB. Effects of soil–structure interaction on real time dynamic response of offshore wind turbines on monopiles. Eng Struct 2014;75:388–401.
[14] Shi S, Zhai E, Xu C, Iqbal K, Sun Y, Wang S. Influence of pile-soil interaction on dynamic properties and response of offshore wind turbine with monopile foundation in sand site. Appl Ocean Res 2022;126:103279.
[15] Liang F, Yuan Z, Liang X, Zhang H. Seismic response of monopile-supported offshore wind turbines under combined wind, wave and hydrodynamic loads at scoured sites. Comput Geotech 2022;144:104640.
[16] Zuo H, Bi K, Hao H. Dynamic analyses of operating offshore wind turbines including soil-structure interaction. Eng Struct 2018;157:42–62.
[17] Kjørlaug RA, Kaynia AM. Vertical earthquake response of megawatt-sized wind turbine with soil-structure interaction effects. Earthq Eng Struct Dyn 2015;44(13):2341–58.
[18] Kementzetzidis E, Corciulo S, Versteijlen WG, Pisanò F. Geotechnical aspects of offshore wind turbine dynamics from 3D non-linear soil-structure simulations. Soil Dyn Earthq Eng 2019;120:181–99.
[19] Jalbi S, Bhattacharya S. Closed form solution for the first natural frequency of offshore wind turbine jackets supported on multiple foundations incorporating soil-structure interaction. Soil Dyn Earthq Eng 2018;113:593–613.
[20] Alati N, Failla G, Arena F. Seismic analysis of offshore wind turbines on bottom-fixed support structures. Phil Trans R Soc A 2015;373(2035):20140086.
[21] Plodpradit P, Dinh VN, Kim K-D. Coupled analysis of offshore wind turbine jacket structures with pile-soil-structure interaction using FAST v8 and X-SEA. Appl Sci 2019;9(8):1633.
[22] Ju S-H, Hsieh C-H. Optimal wind turbine jacket structural design under ultimate loads using Powell's method. Ocean Eng 2022;262:112271.
[23] Gelagoti FM, Kourkoulis RS, Georgiou IA, Karamanos SA. Soil–structure interaction effects in offshore wind support structures under seismic loading. J Offshore Mech Arct Eng 2019;141(6).
[24] Jonkman J, Butterfield S, Musial W, Scott G. Definition of a 5-MW reference wind turbine for offshore system development. Technical report, National Renewable Energy Lab.(NREL), Golden, CO (United States); 2009.
[25] Bossanyi EA. Bladed for windows user manual. Bristol, UK.; 2000.
[26] Abhinav KA, Saha N. Coupled hydrodynamic and geotechnical analysis of jacket offshore wind turbine. Soil Dyn Earthq Eng 2015;73:66–79.
[27] Abhinav KA, Saha N. Nonlinear dynamical behaviour of jacket supported offshore wind turbines in loose sand. Mar Struct 2018;57:133–51.
[28] Jalbi S, Bhattacharya S. Concept design of jacket foundations for offshore wind turbines in 10 steps. Soil Dyn Earthq Eng 2020;139:106357.
[29] Jalbi S, Nikitas G, Bhattacharya S, Alexander N. Dynamic design considerations for offshore wind turbine jackets supported on multiple foundations. Mar Struct 2019;67:102631.
[30] Mo R, Cao R, Liu M, Li M. Effect of ground motion directionality on seismic dynamic responses of monopile offshore wind turbines. Renew Energy 2021;175:179–99.
[31] Mo R, Cao R, Liu M, Li M, Huang Y. Seismic fragility analysis of monopile offshore wind turbines considering ground motion directionality. Ocean Eng 2021;235:109414.
[32] National Renewable Energy Laboratory. OpenFAST documentation. Release v3.4.1. 2023, https://openfast.readthedocs.io/en/main/. Code published at https://github.com/OpenFAST/openfast.
[33] Ju S-H, Huang Y-C. Analyses of offshore wind turbine structures with soil-structure interaction under earthquakes. Ocean Eng 2019;187:106190.
[34] James M, Haldar S. Seismic vulnerability of jacket supported large offshore wind turbine considering multidirectional ground motions. Structures 2022;43:407–23.
[35] Mroczek MM, Arwade SR, Lackner MA. Design optimization of offshore wind jacket piles by assessing support structure orientation relative to metocean conditions. Wind Energy Sci 2023;8(5):807–17, URL https://wes.copernicus.org/articles/8/807/2023/.
[36] Vorpahl F, Popko W, Kaufer D. Description of a basic model of the "UpWind reference jacket" for code comparison in the OC4 project under IEA Wind Annex XXX. Fraunhofer Institute for Wind Energy and Energy System Technology (IWES), Germany 450; 2011.
[37] Jonkman J, Musial W. Offshore code comparison collaboration (OC3) for IEA Wind Task 23 offshore wind technology and deployment. 2010.
[38] IEC. 61400-3-1:2021 wind energy generation systems - Part 3-1: Design requirements for fixed offshore wind turbines. International Electrotechnical Commission; 2021.
[39] DNV. Loads and site conditions for wind turbines. Offshore standard DNV-ST-0437. DetNorske Veritas AS; 2016.
[40] Zhang Q, Zheng XY. Offshore earthquake ground motions: Distinct features and influence on the seismic design of marine structures. Mar Struct 2019;65:291–307.
[41] Pacific Earthquake Engineering Research Center (PEER)2022. NGA-West2 Ground Motion Database. 2022, Available online: ngawest2.berkeley.edu/. [Accessed on 20 November 2022].
[42] National Research Institute for Earth Science and Disaster Resilience (K-NET)2022. Strong-motion seismograph networks. 2022, Available online: https://www.kyoshin.bosai.go.jp/. [Accessed on 20 November 2022].
[43] ISO 19901-2. International Organization for Standardization. ISO 19901-2:2022 Petroleum and natural gas industries — Specific requirements for offshore structures — Part 2: Seismic design procedures and criteria. 2022.
[44] Damiani R, Jonkman J, Hayman G. SubDyn user's guide and theory manual. Technical report, National Renewable Energy Lab.(NREL), Golden, CO (United States); 2015.
[45] Clough RW, Penzien J. Dynamics of structures. 3rd ed.. Computers & Structures; 1995.
[46] Romero-Sánchez C, Padrón LA. An implementation of multi-support input motion into openfast for the earthquake analysis of offshore wind turbines. Eccomas Proceedia COMPDYN 2023;172–85, URL https://www.eccomasproceedia.org/conferences/thematic-conferences/compdyn-2023/10396.
[47] Carbonari S, Morici M, Dezi F, Leoni G. A lumped parameter model for time-domain inertial soil-structure interaction analysis of structures on pile foundations. Earthq Eng Struct Dyn 2018;47(11):2147–71.
[48] Romero-Sánchez C, Padrón LA. Implementation of ground input motion and dynamic soil-structure interaction into openfast for the seismic analysis of offshore wind turbines. In: Congress on numerical methods in engineering. International Center for Numerical Methods in Engineering (CIMNE); 2022.

[49] Chopra AK. Dynamics of structures. Theory and applications to earthquake engineering. 7th ed.. Pearson; 2017.
[50] Álamo GM, Bordón JDR, Aznárez JJ. On the application of the beam model for linear dynamic analysis of pile and suction caisson foundations for offshore wind turbines. Comput Geotech 2021;134:104107.
[51] Dobry R, Idriss IM, Ng E. Duration characteristics of horizontal components of strong-motion earthquake records. Bull Seismol Soc Am 1978;68(5):1487–520.
[52] Arias A, Hansen R. Seismic design for nuclear power plants. Measure Earthq Intensity 1970;438–83.